Accepted Manuscript
Version of record at: https://doi.org/10.3847/2041-8213/ac21d2

von Karman Correlation Similarity of the Turbulent Interplanetary Magnetic Field

Sohom Roy[1] , R. Chhiber[1,2], S. Dasso[3,4], M. E. Ruiz[5], and W. H. Matthaeus[1,6]

[1] Department of Physics and Astronomy, University of Delaware, Newark, DE, USA
[2] Heliophysics Science Division, NASA Goddard Space Flight Center, Greenbelt, MD, USA
[3] CONICET, Universidad de Buenos Aires, Instituto de Astronomía y Física del Espacio, LAMP Group, CC. 67, Suc. 28, 1428 Buenos Aires, Argentina
[4] Universidad de Buenos Aires, Facultad de Ciencias Exactas y Naturales, Departamento de Ciencias de la Atmósfera y los Océanos and Departmento de Física, LAMP Group, 1428 Buenos Aires, Argentina
[5] Servicio Meteorológico Nacional, Av. Dorrego 4019—CABA República Argentina (C1425GBE) and Instituto de Astronomía y Física del Espacio (IAFE) and Departamento de Física, Facultad de Ciencias Exactas y Naturales, Universidad de Buenos Aires, Buenos Aires, Argentina
[6] Bartol Research Institute, University of Delaware, Newark, DE, USA; whm@udel.edu; sohom@udel.edu
© 2021. The American Astronomical Society. All rights reserved.

Abstract

A major development underlying much of hydrodynamic turbulence theory is the similarity decay hypothesis due to von Karman and Howarth here extended empirically to magnetic field fluctuations in the solar wind. In similarity decay the second-order correlation experiences a continuous transformation based on a universal functional form and a rescaling of energy and characteristic length. Solar wind turbulence follows many principles adapted from classical fluid turbulence, but previously this similarity property has not been examined explicitly. Here we analyze an ensemble of magnetic correlation functions computed from Advanced Composition Explorer data at 1 au, and demonstrate explicitly that the two-point correlation functions undergo a collapse to a similarity form of the type anticipated from von Karman's hypothesis. This provides for the first time a firm empirical basis for employing the similarity decay hypothesis to the magnetic field, one of the primitive variables of magnetohydrodynamics, and one frequently more accessible from spacecraft instruments. This approach is of substantial utility in space turbulence data analysis, and for adopting von Karman-type heating rates in global and subgrid-scale dynamical modeling.

1. Introduction

Several fundamental building blocks of modern turbulence theory emerge from the von Karman–Howarth treatment of turbulent energy decay in hydrodynamics (de Kármán & Howarth 1938). A prominent step is the development of equations for the time evolution of the second-order (two-point, single-time) correlation functions. These so-called von Karman–Howarth equations are the first entry in the hierarchy of moment equations and form the basis of the famous Kolmogorov "4/5" (or third-order) law for evaluating the energy cascade rate (Kolmogorov 1941a). Another important concept that is introduced in the same work is that of *self-preservation* of the two-point correlations during decay. The conjecture is that the dynamical behavior of the correlation function over a suitable intermediate range of spatial separations, or lags, depends only on a small number of similarity variables; for hydrodynamics the number is two—the energy per unit mass u^2, and a single similarity length-scale λ. Normalized in an appropriate way, the underlying dimensionless correlation function takes on a quasi-universal form over the relevant range of length scales. This formalism then implies a familiar decay law for the large, energy-containing length scales, setting the stage for control of the entire turbulence cascade process by the large-scale energy reservoirs. The experimental confirmation of the validity of this picture, up to a suitable degree of accuracy, is a cornerstone of hydrodynamic turbulence theory (Batchelor & Townsend 1947, 1948; Stewart & Townsend 1951; Batchelor 1970; Pope 2000). The scope of potential applications of the von Karman–Howarth ideas extends much further, and has been expounded for magneto-hydrodynamics (MHD) and for plasmas with some support, mainly from numerical simulations (Hossain et al. 1995; Wu et al. 2013; Bandyopadhyay et al. 2018). Extrapolating to natural systems there is a strong motivation to apply, and if possible to validate, the von Karman approach in observations of turbulence.

Here, we evaluate directly the self-preservation hypothesis for magnetic autocorrelation functions observed at 1 au in the turbulent solar wind. We emphasize that the magnetic field and velocity field are equally primitive variables for incompressible MHD and a more complete analysis would examine both or, equivalently, the Elsässer (1950) fields. Our choice to examine the magnetic field alone has a practical basis in that the magnetic field is often better determined by standard spacecraft instrumentation. Consequently the magnetic fluctuation properties have often been used as a surrogate for the full Kolmogorov cascade, as frequently seen in the emphasis on the magnetic field spectrum as a separate entity (Kiyani et al. 2015). This test employs a large ensemble of samples of solar wind magnetic field data of sufficient size to separately compute correlation lengths and energy densities for each sample. Carrying out the two-stage normalization prescribed in the von Karman procedure, we find a collapse of the correlation functions to a well-defined form. This provides for the first time a direct confirmation of von Karman similarity for an extraterrestrial space plasma.

2. von Karman Normalization

For simplicity and to make contact with theory, we assume that the solar wind magnetic field can be expressed as the sum

Accepted Manuscript
Version of record at: https://doi.org/10.3847/2041-8213/ac21d2

of the mean magnetic field, and a fluctuation term:

$$\boldsymbol{B}(\boldsymbol{x}, t) = \overline{\boldsymbol{B}}(\boldsymbol{x}, t) + \boldsymbol{b}(\boldsymbol{x}, t), \quad (1)$$

where $\overline{\boldsymbol{B}}(\boldsymbol{x}, t)$ is the mean magnetic field, and $\boldsymbol{b}(\boldsymbol{x},t)$ is the fluctuation in the magnetic field. An ensemble average $\langle ... \rangle$ defines this decomposition as $\langle \boldsymbol{B} \rangle = \overline{\boldsymbol{B}}$ and $\langle \boldsymbol{b} \rangle = 0$. The two-point, single-time correlation function is defined as

$$R(\boldsymbol{r}, t) = \langle \boldsymbol{b}(\boldsymbol{x}, t) \cdot \boldsymbol{b}(\boldsymbol{x} + \boldsymbol{r}, t) \rangle. \quad (2)$$

Homogeneity implies that this quantity depends only on the spatial lag $\boldsymbol{r}$ and is independent of $\boldsymbol{x}$ (Batchelor 1970; Matthaeus & Goldstein 1982). Note that here we are not assuming stationarity in time, as we are considering turbulence that freely decays in time t. The associated systematic time variation is described by the von Karman hypothesis outlined below. The present theoretical discussion is readily generalized to a correlation tensor $R_{ij}(\boldsymbol{r})$; we forgo this generalization here for brevity. A familiar assumption (de Kármán & Howarth 1938) is that of statistical isotropy, that is, invariance of the correlations under rotations, so that R depends only on the magnitude r of the spatial lag $\boldsymbol{r}$. Alternatively, the theory may be generalized for anisotropic cases (Wan et al. 2012; as expected for the solar wind) by introducing length scales parallel and perpendicular to the magnetic field direction. Here we adopt an ensemble that includes samples for all available directions; by broadening the averaging procedure to sum over all directions, we arrive at a functional representation that is "omnidirectional" (Batchelor 1970) and depends on a single spatial lag.

The von Karman similarity assumption, adapted to the magnetic field, proceeds by analogy to the hydrodynamic case as follows. Suppose that during free turbulent decay the energy density (per unit mass) of the magnetic field, expressed in Alfvén speed units and up to a factor of 2, varies in time as $u^2(t) \equiv \langle v_A^2(t) \rangle$ where $v_A^2 = |\boldsymbol{b}(t)|^2/(4\pi\rho)$, where ρ is a suitably coarse-grained mass density (Parashar et al. 2020). We denote the variance of the measured magnetic field (in nT^2) as $b^2(t)$.

A time-varying characteristic length $L(t)$ along with the characteristic time $\tau(t) = L(t)/u(t)$ comprise the similarity variables that describe the von Karman turbulent decay. The length L will often be associated with the outer scale or correlation scale of the fluctuations. There are at least two potential implications of the similarity variables $L(t)$ and $\tau(t)$: First, during free decay the equations can be written in terms of these variables. In so doing it is possible that semi-universal decay solutions can be written that do not involve the laboratory time or length, but only the dimensionless variables t/τ and r/L. The auxiliary constraint conditions for this *similarity solution* are the well-known von Karman decay laws $\frac{du^2}{dt} = -\alpha u^3/L$ and $\frac{dL}{dt} = \beta u$. These are quite well established for both hydrodynamics and MHD (Hossain et al. 1995; Bandyopadhyay et al. 2018) with some support for weakly collisional plasmas (Wu et al. 2013). If such solutions exist and are realized in nature, then a consequence (or corollary) is that the correlation functions themselves undergo a continuous time-dependent renormalization with respect to these variables such that the conditions for similarity decay are maintained. Below we verify the approximate validity of this *self-preservation* property for the turbulent interplanetary magnetic field.

To be specific, the von Karman similarity hypothesis asserts that the functional form of the two-point correlation function is *self-preserving* in the sense that at any stage of the decay it can be expressed as

$$R(r, t) = u^2(t)\hat{R}(r/L(t)). \quad (3)$$

Here $\hat{R}$ is a universal function that describes the dynamics of the correlation function over a range of scales r that is much larger than the dissipative scales, and smaller than any specific structures at scales associated with injection of energy. There is, of course, no guarantee that physically realizable correlation functions will collapse to this form upon appropriate normalization. This must be established empirically. We proceed below to test this approximate collapse to a near-universal form using magnetic field data at 1 au.

In addition to assessing the quality of the von Karman normalizations for the correlation functions, we carry out the analogous procedure for the second-order magnetic structure functions:

$$S^{(2)}(\boldsymbol{r}, t) = \langle (\boldsymbol{b}(\boldsymbol{x} + \boldsymbol{r}, t) - \boldsymbol{b}(\boldsymbol{x}, t))^2 \rangle, \quad (4)$$

a quantity that occupies a prominent role in Kolmogorov's seminal theories (Kolmogorov 1941a, 1941b; Frisch 1995; Pope 2000). Following Equation (3) the normalized second-order structure function, assuming isotropy or direction-averaging, may be written as

$$S^{(2)}(r, t) = u^2(t)\hat{S}(r/L(t)). \quad (5)$$

3. Data and Analysis Procedure

Ensemble of data at 1 au. The data used to compute the correlation functions are Advanced Composition Explorer (ACE) Level 2 MAG data (Smith et al. 1998) at 1 s resolution, which were then downsampled to 1 minute cadence. The data span a range of 10 years, from 1998 February 5 to 2008 March 30, consisting of 1 day intervals, in total comprising approximately 3000 samples after discarding cases that included excessive missing data or bad values. In the present Letter the analysis is restricted to fast wind samples that we define to be those with average wind speeds $>500\,\mathrm{km\,s^{-1}}$; this reduced the ensemble size to 987 samples. Data sets were cleaned by replacing missing or bad data points with NaN values.

The correlation functions are estimated from each data set (with label I) using the *Blackman–Tukey* algorithm (Blackman & Tukey 1958), implemented at this stage in the time domain with τ denoting the time lag:

1. The magnetic field is given by B_i (components $i = 1, 2, 3$). For a given lag τ, two sets of arrays are created, $\boldsymbol{B}_\mathrm{l}$ (the *left* array) and $\boldsymbol{B}_\mathrm{r}$ (the *right* array), which are defined as

$$B_{i,\mathrm{l}} = B_i[0\colon L - \tau], \quad B_{i,\mathrm{r}} = B_i[\tau\colon L], \quad (6)$$

where L is the length of the entire data set, and i takes on the values R, T, and N, representing coordinates in a Sun-centered coordinate system (Fränz & Harper 2002). In the usual way, the square brackets denote a range of indices within the data set.

Accepted Manuscript
Version of record at: https://doi.org/10.3847/2041-8213/ac21d2

2. Then the following equation is used to compute the correlation tensor for the given lag:

$$R_{ij}(\tau) = \langle B_{i,\mathrm{l}} B_{j,\mathrm{r}} \rangle - \langle B_{i,\mathrm{l}} \rangle \langle B_{j,\mathrm{r}} \rangle, \quad (7)$$

where $\langle M \rangle$ denotes averaging over the entire length of the array M.

3. Then the autocorrelation is computed using the following equation:

$$R(\tau) = R_{\mathrm{RR}}(\tau) + R_{\mathrm{TT}}(\tau) + R_{\mathrm{NN}}(\tau). \quad (8)$$

4. At this stage time lags are converted to spatial lags using the Taylor frozen-in hypothesis (Taylor 1938):

$$r = V_{\mathrm{sw}} \tau, \quad (9)$$

where V_{sw} is the mean solar wind speed for interval I, and r is a spatial lag in the radial direction.

We then proceed to apply the normalizations described by Equation (3) to the collection of intervals. Operationally, we compute the correlation length λ_I and average magnetic energy per unit mass $u_I^2 \equiv R_I(0)$ for each sampled interval. Each correlation function (labeled by interval I) is self-normalized as $R_I(r/\lambda_I)/R_I(0)$. Then these are averaged over all I to obtain an estimate of the quasi-universal $\hat{R}(r/\lambda)$. The average correlations are compared with the individually normalized correlations in the figures below. Note that a median is used to represent the average at each lag.

The twice-normalized second-order structure function estimates are obtained similarly as

$$\frac{S_I^{(2)}(r/\lambda_I)}{R_I(0)} = 2\frac{R_I(0) - R_I(r/\lambda_I)}{R_I(0)}. \quad (10)$$

Then the average over intervals produces the estimate of $\hat{S}^{(2)}(r/\lambda)$.

4. Normalizations and Results

Figure 1 (top) illustrates the range of unnormalized correlation functions as a function of unnormalized spatial lag in km. We have used boxplots to illustrate the distribution of the correlation functions at each stage in the normalization procedure. The solid line shows the median of the correlation functions at each (binned) lag, and the upper and lower boundaries of the boxes describe the first (Q1) and the third (Q3) quartiles. The whiskers of the boxplot show the "minimum" and "maximum" values of the correlations, which are defined with respect to the interquartile range, IQR = (Q3–Q1):

$$\mathrm{min} = \mathrm{Q1} - 1.5{*}\mathrm{IQR}, \quad \mathrm{max} = \mathrm{Q3} + 1.5{*}\mathrm{IQR}. \quad (11)$$

The first normalization is accomplished by the procedure $R_I(r) \rightarrow R_I(r)/R_I(0)$ for each interval labeled by I. The correlation functions are interpolated onto a uniform grid. The median is then computed for the ensemble of correlation functions at each grid point, along with the "minimum" and "maximum" values as described above. The result, which we call the first-normalized correlation function, is plotted in the middle panel of Figure 1 as the median value. The boxes give us an estimation of the spread in the population of $R_I(r)/R_I(0)$ values; it is evident that the distribution is skewed.

The next step is to compute correlation scales λ_I for each sample. The method employed is a composite of two approaches implemented in previous studies (Ruiz et al. 2014; Isaacs et al. 2015). From the Blackman–Tukey autocorrelations computed above a preliminary estimate of λ_I is obtained by computing the "1/e" length, that is the length λ_I' for which $R_I(\lambda_I')/R_I(0) = 1/e = 0.3678\ldots$. Finally, a linear least-squares fit to $\log[R_I(\ell)/R_I(0)] \sim -\ell/\lambda_I$ is performed over the interval $r = (0, \lambda_I'/2)$ to obtain λ_I.

The fit determines λ_I for the Ith sample. The argument of the correlation can then be scaled to ℓ/λ_I as in Equation (3). Computing the medians over the population of rescaled correlations produces the second-normalized correlation functions. The median second-normalized correlation function is portrayed in the bottom panel of Figure 1, along with the boxes indicating the first and third quartiles of the population, and the whiskers showing the "minimum" and "maximum" values.

By comparison of the three panels in Figure 1, it is clear that each normalization produces a significant reduction of statistical spread of the population of correlation functions. This effect is particularly dramatic for lags less than a correlation scale. A quantitative measure of this collapse to a well-defined median is provided in Table 1, which shows the properly normalized standard deviations of the populations in the unnormalized population and in the first- and second-normalized populations. In Appendix appendix, we show the distributions of the fluctuation energies, the distribution of the correlation lengths, and the distribution of the second-normalized correlation functions at $r = \lambda$.

This collapse of the correlations is a standard approach to demonstrating the applicability of turbulence theory to data (Batchelor 1970; Pope 2000) and in this case provides an empirical confirmation of the applicability of von Karman similarity to interplanetary magnetic field observations.

An entirely analogous procedure may be applied to normalize the second-order structure functions. We briefly show the results here for completeness. Applying the relationship Equation (10) between $S_I^{(2)}$ and R_I, for each data interval I, and then averaging over the set of intervals, we arrive at the average $\hat{S}^2(r/\lambda)$ as in Equation (5).

Shown in Figure 2 are the results of double normalization of the structure functions for the same 987 fast wind samples extracted from the ACE ensemble. Both dimensionless structure function and dimensionless length r/λ are on a linear scale. $\hat{S}^{(2)}$ is shown as a solid line, representing the median of the underlying estimates. The distribution of the population is suggested by the background samples and shading at the first and third quartiles about the median structure function. It is apparent that at lags $r/\lambda < 1$ there is a substantial collapse to what might be loosely thought of as a "universal form." At large lags $r/\lambda \gg 1$ the population tends toward the asymptotic value of 2, which is achieved only when the sampled fluctuations become entirely uncorrelated. Another view, on a log–log scale, of the normalized structure function is provided in Figure 3. This rendition emphasizes the inertial range. A line with 2/3 slope is provided for reference, representing the expected inertial range scaling of $S^{(2)} \sim r^{2/3}$ in K41 theory.

5. Discussion

The von Karman similarity decay hypothesis is the basis for phenomenological treatments of turbulence decay of the form

$$\text{decay rate} \propto \frac{(\text{velocity})^3}{\text{similarity scale}}. \quad (12)$$

Accepted Manuscript
Version of record at: https://doi.org/10.3847/2041-8213/ac21d2

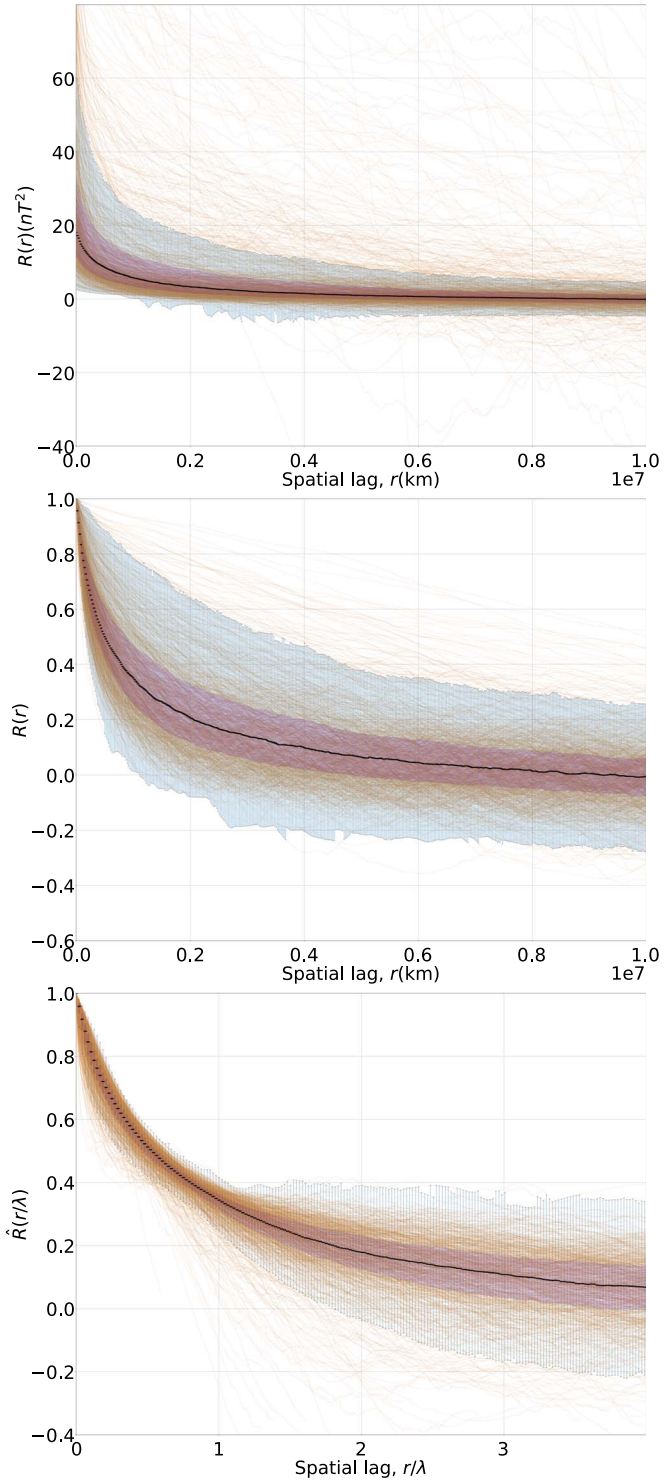

Figure 1. (top) Correlation functions not normalized. The solid black line shows the median correlation vs. lag. The upper and lower boundaries of the (brown) boxes indicate the first and third quartiles, respectively, at each grid point. The whiskers extending from the boxes denote the "minimum" and "maximum" values as described in Section 4. To produce these boxplots, the data are interpolated and resampled onto a grid of 48 points per 10^6 km span of lag. (middle) Correlation functions after first normalization—normalization by energy. (bottom) Correlation functions normalized by energy and correlation scale.

Along with a formulation for evolution of the similarity scale, relations of this form emerge in both hydrodynamics and MHD as conditions for maintaining the property of *self-preservation*

Table 1
Standard Deviations of Correlation Functions, Scaled as $\sigma/R(0)$, for Different Stages of Normalization at Selected Values of Lags

	$r/\lambda = 0.25$	$r/\lambda = 0.5$	$r/\lambda = 1$
No normalization	2.163	2.015	1.759
First normalization	0.106	0.139	0.157
Second normalization	0.032	0.022	0.055

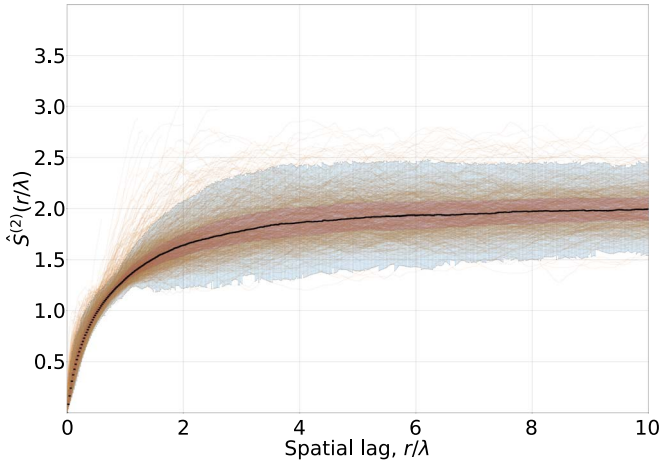

Figure 2. Normalized second-order structure functions vs. lag, on a linear scale. See Figure 1 for a description of the boxplot elements.

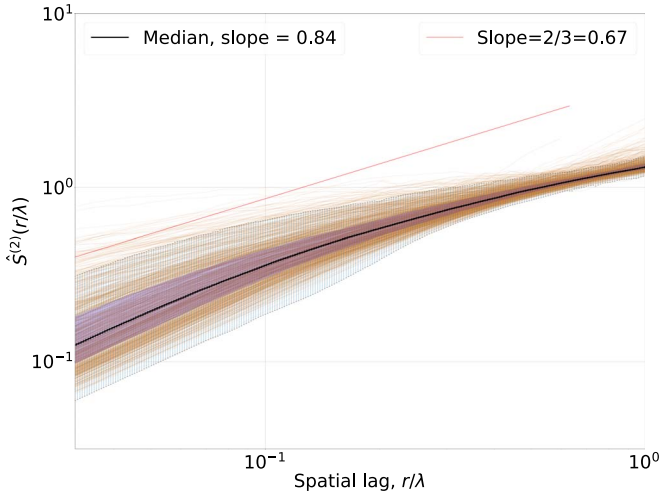

Figure 3. Normalized second-order structure functions on a log–log scale. A linear fit has been performed on the median for lags less than 0.5 correlation length.

of the functional form of the second- and third-order correlation functions during decay of the turbulence. In particular, for MHD, a model most frequently applied to the large scale and inertial range scales of the solar wind (Matthaeus & Goldstein 1982; Bruno & Carbone 2013), the appropriate generalization is the assumption of self-preservation of the Elsässer correlation functions (Oughton et al. 1997) or, equivalently, the total incompressive fluctuation energy—kinetic plus magnetic —as well as the cross correlation of velocity and magnetic field. For details see Wan et al. (2012). For the leading-order description, in incompressible MHD, the condition for

Accepted Manuscript
Version of record at: https://doi.org/10.3847/2041-8213/ac21d2

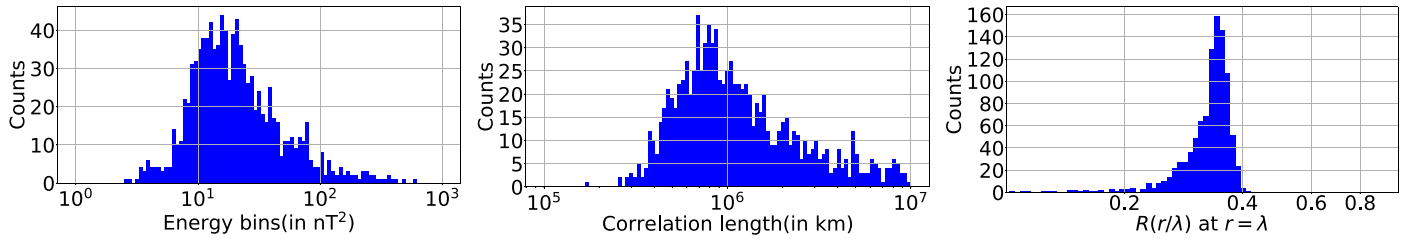

Figure 4. (left) Distribution of energies before normalizations. (middle) Distribution of correlation lengths. (right) Distribution of correlations at 1 correlation length, after two normalizations.

obtaining these self-preservation conditions, which are generalizations of Equation (3), are shown to be

$$\frac{dZ_{\pm}^2}{dt} = -\alpha_{\pm}\frac{Z_{\pm}^2 Z_{\mp}}{L_{\pm}}; \quad \frac{dL_{\pm}}{dt} = \beta_{\pm} Z_{\mp}. \tag{13}$$

The present results provide significant conceptual support for use of similarity decay laws of the von Karman type as a representation of the dissipation and heating due to turbulence cascade (Hossain et al. 1995). This approach and its variations are extensively employed in space physics applications, including turbulence transport equations (Matthaeus et al. 1994; Breech et al. 2008; Adhikari et al. 2017) and both coronal (Cranmer et al. 2007; Verdini et al. 2010) and heliospheric (Lionello et al. 2014; van der Holst et al. 2014; Usmanov et al. 2018) global models that include subgrid turbulence effects.

The above analysis affirms that an isotropic form of the von Karman self-preservation hypothesis is applicable, at a reasonable level of approximation, for solar wind magnetic field fluctuations in fast wind at 1 au in near-Earth orbit. In stating the hypothesis in this form we extend the ideas of von Karman and Howarth in several important ways. First, we examine the similarity hypothesis for the magnetic field fluctuations alone. In so doing we ignore the velocity field fluctuations, which one would normally view as entering on equal footing, given that the incompressible energy in the turbulence is the sum of magnetic and velocity field contributions. Second, density fluctuations are also ignored in this analysis, with the understanding that the incompressive fluctuation energy is the dominant ingredient of the turbulence (Matthaeus et al. 1990). Finally, we also adopt an extended hypothesis that the similarity form implied by Equation (3) can be obtained after averaging over directions, even though the solar wind is known to be anisotropic (Matthaeus et al. 1990; Dasso et al. 2005). The legitimacy of this procedure is formally established for the related third-order law in anisotropic hydrodynamics (Nie & Tanveer 1999; Taylor et al. 2003); we view it as a plausible assumption that a similar procedure can be carried out for anisotropic MHD, as a justification for application to the (manifestly) anisotropic solar wind plasma (Bruno & Carbone 2013).

Further examination of the issue of anisotropy will be deferred to a subsequent report. The present focus on the magnetic field is also a conceptual shortcoming, even though magnetic field is often adopted as a surrogate for the full Kolmogorov cascade; however, it will clearly be a priority to extend the present similarity analysis to the full Elsässer variables, taking velocity fields into account.

In this preliminary report we analyzed only the fast wind, in order to not confuse different wind types that may systematically differ. Future work will study the properties of the full ensemble of correlations including slow wind, fast wind, and their comparison. Finally, to the extent that the present demonstration stands on firm footing, it may further motivate implementation of von Karman similarity to a wider variety of astrophysical applications (Elmegreen & Scalo 2004).

This research supported in part by NASA Heliophysics Supporting Research grants 80NSSC18K1210 and 80NSSC18K1648, NASA Heliophysics Guest Investigator grant 80NSSC19K0284, and the NASA IMAP project under subcontract SUB0000317 from Princeton University, and the NASA PUNCH project under SWRI subcontract N99054DS. SD acknowledges partial support from the Argentinean grants UBACyT (UBA). The ACE magnetic field data were downloaded from https://spdf.gsfc.nasa.gov/pub/data/ace/mag/level_2_cdaweb/mfi_h3.

Appendix A
Distributions

This material provides additional information concerning the distribution of energies and correlation lengths in the fast wind sample from the ACE magnetic field instrument discussed in the main text. It also shows a distribution of estimates of the normalized correlation at a one correlation length lag.

The following figures show the distributions of the energies and the correlation lengths, which are the two quantities that characterize the two stages of our normalization. Additionally, the distribution of the magnetic field autocorrelation functions, after applying the two normalizations mentioned above, are shown at 1 correlation length.

From Figure 4, we can see that there is a wide variability in the magnetic field energies, as well as the correlation lengths. But, after normalizing as per the von Karman procedure, we see that the distribution of the correlation functions at 1 correlation length has a very narrow spread.

ORCID iDs

Sohom Roy https://orcid.org/0000-0003-3891-5495
R. Chhiber https://orcid.org/0000-0002-7174-6948
S. Dasso https://orcid.org/0000-0002-7680-4721
W. H. Matthaeus https://orcid.org/0000-0001-7224-6024

References

Adhikari, L., Zank, G. P., Hunana, P., et al. 2017, ApJ, 841, 85
Bandyopadhyay, R., Oughton, S., Wan, M., et al. 2018, PhRvX, 8, 041052
Batchelor, G. K. 1970, The Theory of Homogeneous Turbulence (Cambridge: Cambridge Univ. Press)
Batchelor, G. K., & Townsend, A. A. 1947, RSPSA, 190, 534
Batchelor, G. K., & Townsend, A. A. 1948, RSPSA, 193, 539
Blackman, R. B., & Tukey, J. W. 1958, Bell Syst. Tech. J., 37, 185
Breech, B., Matthaeus, W. H., Minnie, J., et al. 2008, JGR, 113, A08105

Accepted Manuscript
Version of record at: https://doi.org/10.3847/2041-8213/ac21d2

Bruno, R., & Carbone, V. 2013, LRSP, 10, 2
Cranmer, S. R., van Ballegooijen, A. A., & Edgar, R. J. 2007, ApJS, 171, 520
Dasso, S., Milano, L. J., Matthaeus, W. H., & Smith, C. W. 2005, ApJL, 635, L181
de Kármán, T., & Howarth, L. 1938, RSPSA, 164, 192
Elmegreen, B. G., & Scalo, J. 2004, ARA&A, 42, 211
Elsässer, W. M. 1950, PhRv, 79, 183
Fränz, M., & Harper, D. 2002, Plan. Sp. Sci., 50, 217
Frisch, U. 1995, Turbulence (Cambridge: Cambridge Univ. Press)
Hossain, M., Gray, P. C., Pontius, D. H., Jr., Matthaeus, W. H., & Oughton, S. 1995, PhFl, 7, 2886
Isaacs, J. J., Tessein, J. A., & Matthaeus, W. H. 2015, JGRA, 120, 868
Kiyani, K. H., Osman, K. T., & Chapman, S. C. 2015, RSPTA, 373, 20140155
Kolmogorov, A. N. 1941a, C.R. Acad. Sci.U.R.S.S., 31, 538
Kolmogorov, A. N. 1941b, Dokl. Akad. Nauk SSSR, 30, 301
Lionello, R., Velli, M., Downs, C., et al. 2014, ApJ, 784, 120
Matthaeus, W. H., & Goldstein, M. L. 1982, JGR, 87, 6011
Matthaeus, W. H., Goldstein, M. L., & Roberts, D. A. 1990, JGR, 95, 673
Matthaeus, W. H., Oughton, S., Pontius, D., & Zhou, Y. 1994, JGR, 99, 267
Nie, Q., & Tanveer, S. 1999, RSPSA, 455, 1615
Oughton, S., Rädler, K.-H., & Matthaeus, W. H. 1997, PhRvE, 56, 2875
Parashar, T., Goldstein, M., Maruca, B., et al. 2020, ApJS, 246, 58
Pope, S. B. 2000, Turbulent Flows (Cambridge: Cambridge Univ. Press)
Ruiz, M. E., Dasso, S., Matthaeus, W. H., & Weygand, J. M. 2014, SoPh, 289, 3917
Smith, C. W., L'Heureux, J., Ness, N. F., et al. 1998, SSRv, 86, 613
Stewart, R. W., & Townsend, A. A. 1951, RSPTA, 243, 359
Taylor, G. I. 1938, RSPSA, 164, 476
Taylor, M. A., Kurien, S., & Eyink, G. L. 2003, PhRvE, 68, 026310
Usmanov, A. V., Matthaeus, W. H., Goldstein, M. L., & Chhiber, R. 2018, ApJ, 865, 25
van der Holst, B., Sokolov, I. V., Meng, X., et al. 2014, ApJ, 782, 81
Verdini, A., Velli, M., Matthaeus, W. H., Oughton, S., & Dmitruk, P. 2010, ApJL, 708, L116
Wan, M., Oughton, S., Servidio, S., & Matthaeus, W. H. 2012, JFM, 697, 296
Wu, P., Wan, M., Matthaeus, W. H., Shay, M. A., & Swisdak, M. 2013, PhRvL, 111, 121105